AMERICAN SCIENTIFIC PUBLISHERS

Journal of Nanofluids
Vol. 6, pp. 1–10, 2017
(www.aspbs.com/jon)

ARTICLE

Hydromagnetic Boundary Layer Slip Flow of Nanofluid Through Porous Medium Over a Slendering Stretching Sheet

R. V. M. S. S. KiranKumar and S. V. K. Varma*

Department of Mathematics, S. V. University, Tirupati 517502, A.P, India

The magnetohydrodynamic boundary layer slip flow behavior of a nanofluid over a slendering stretching surface through a porous medium with thermal radiation, viscous dissipation and first order chemical reaction is numerically investigated. The model used for the nanofluid incorporates the effects of thermophoresis and Brownian motion. With the aid of similarity variables, the governing equations are transformed into a set of coupled non-linear ordinary differential equations (ODE's) and then solved numerically by using boundary value problem default solver in MATLAB bvp4c package. The impact of important parameters on the fluid properties as well as on the friction factor coefficient, reduced local Nusselt number and reduced local Sherwood number are determined. To confirm the numerical method, comparisons are made with the existing results in the text for some special cases and the results are found to be in outstanding agreement. Further, it is found that the velocity slip parameter controls the heat transfer rate.

KEYWORDS: Slendering Stretching Sheet, Porous Medium, Magneticfield, Chemical Reaction, Thermal Radiation.

1. INTRODUCTION

The study of heat transfer flow in boundary layer over a stretching sheet has concerned many researchers because of its abundant practical applications, for example, in metallurgical processes, such as continuous filaments drawing through quiescent fluids, annealing and tinning of copper wires, glass blowing, built-up of plastic and rubber sheets, crystal growing, continuous cooling and fiber spinning. Moreover, there are wide-ranging of applications in many engineering processes, for example wire drawing, polymer extrusion, continuous casting, manufacturing of foods and paper, glass fiber production, stretching of plastic films, and many others. During the manufacture of these sheets, the melt issues from a slit and is subsequently stretched to achieve the desired thickness. The final product with the desired features strictly depends upon the rate of cooling in the process, the stretching rate, and the process of stretching.

The study of boundary layer flows over a stretching sheet is important as it occurs in several manufacturing process, such as, manufacturing of materials with extrusion. During the manufacturing process, a stretching surface interacts with the ambient fluid both thermally and mechanically. Crane[1] and Dutta et al.[2] considered the dynamics of boundary layer flow over a stretching surface. Practically, the stretching sheet need not be flat. Variable thickness sheet can be encountered more often in real world applications. Plates with variable thickness are often used in machine design, architecture, nuclear reactor technology, naval structures and acoustical components. Variable thickness is one of the important properties in the study of orthotropic plates vibration

The concept of nanofluid is a new class of heat transfer fluids that contain a base fluid and nanoparticles. Nanofluids have been exposed to enhance the thermal conductivity and convective heat transfer performance of the base fluids. One of the possible mechanisms for abnormal increase in the thermal conductivity of nanofluids is the Brownian motions of the nanoparticles inside the base fluids. An inventive way of improving the heat transfer in fluids by suspending tiny solid particles in the fluids was introduced by Choi.[3] This new kind of fluids named as nanofluids which are a suspension of solid nanoparticles of diameter 1–100 nm in conventional heat transfer base fluids for example water, oil or ethylene glycol. It is said that these fluids increase the heat transfer performance of the base fluid enormously. This characteristic aspect of nanofluids is to increase the thermal conductivity which is more useful in cooling rate requirements. Buongiorno[4] presented the comprehensive survey of convective transport by pointing out various facts concerning

*Author to whom correspondence should be addressed.
Email: svijayakumarvarma@yahoo.co.in
Received: 23 February 2017
Accepted: 28 March 2017

nanofluids. Further, he explained the thermal conductive of nanofluids.[5] Angayarkanni and Philip[6] explained the recent progress in nanofluids research from a heat transfer perspective and thermal properties of nanofluids, phase change materials and hybrid nanofluids. Also, he[7] reported the large tunable thermal conductivity in a phase change alkane using inverse micellar templating. Shima and Philip[8] have analyzed the effect of initial thermal conductivity of dispersed nanomaterials on thermal conductivity of nanofluid enhancement of stable nanofluids of Ag and Fe_3O_4 with an average particles size of 7 nm, synthesized by reduction and coprecipitation techniques. Later, the thermal conductivity changes in phase change alkane incorporated with copper nanowire, multiwalled carbon nanotube, and graphene nanoplatelets inclusions with different loadings is considered by Angayarkanni and Philip.[9]

Hamad and Ferdows[10] studied the similarity solution to viscous nanofluid flow and heat transfer effects over a nonlinearly stretching surface. Rana and Bhargava[11] considered the heat transfer flow and of a nanofluid past a nonlinear stretching surface. The boundary layer nanofluid flow over a non-linear permeable stretching surface at prescribed surface temperature with partial slip is examined by Das.[12] Shaw et al.[13] have investigated the nanofluid flow along a permeable surface with conventional no-slip boundary conditions are replaced by slip boundary conditions.

The concept of magnetohydrodynamic has many applications in different fields such as engineering, agriculture and petroleum industries etc. The free convection flow with the effect of a magnetic field has also applications in geophysics and astrophysics.[14] Because of this many studies were performed with the effect of magnetic field. Mabood et al.[15] have investigated the magnetohydrodynamic boundary layer flow a water based nanofluid along a nonlinear stretching sheet with viscous dissipation. Vajravelu et al.[16] have considered the hydrodynamic flow of a conducting fluid past a stretching surface with variable thickness subjected to variable fluid properties. The dissipative magneto-convective flow over a vertical nonlinear stretching surface was considered by Abel et al.[17] Anjali Devi and Prakash[18] scrutinized the impact of thermal conductivity and temperature dependent viscosity on hydromagnetic flow over a slendering stretching sheet.

Boundary layer flow in the presence of porous media can extensively change the flow field and, as a result, affect the heat transfer rate at the surface. Generally, porous media are modeled using the classical Darcy formulation, which implies that the mean filter velocity is relative to the summation of the gravitational force and the pressure gradient. The model is experimental and cannot be derived analytically through a momentum on a small element of porous medium. Yohannes and Sankar[19] have studied the magnetohydrodynamic convective nanofluid flow through a porous media over a stretching sheet with the effects of dissipation, and chemical reaction and thermo-diffusion. Ahmed et al.[20] investigated the nanofluid flow due to a nonlinear stretching sheet in the presence of viscous dissipation. Also, they studied the effect of thermophoresis, Brownian motion and nanoparticle volume fraction in a porous medium. Recently, Prasad et al.[21] investigated the magnetohydrodynamic free convection flow of nanofluid over a vertical porous plate in a rotating frame with variable heat flux.

The radiation effect is very significant particularly at high operating temperatures encountered in the field of space technology. The knowledge of radiative heat transfer has becomes very important, mainly in designing pertinent equipment for use in engineering processes involving high temperatures. Accordingly, recent studies have incorporated the thermal radiation effect. Cortell[22] analyzed the viscous dissipation and thermal radiation effects over a non-linear stretching sheet. Rana et al.[23] studied the magnetohydrodynamic slip flow of a nanofluid due to a permeable stretching/shrinking surface with the effect of thermal radiation. Pal et al.[24] studied the magnetohydrodynamic mixed convection nanofluid flow over a non-linear stretching and shrinking sheets in the presence of thermal radiation and viscous dissipation. Anjali Devi and Prakash[25] studied magnetohydrodynamic flow over a variable thickness stretching sheet in the presence of thermal radiation and they analyzed how the thermal radiation influences the heat transfer rate. Recently, Nagendramma[26] considered the Maxwell nanofluid with slip boundary conditions over a permeable stretching sheet in the presence of thermal radiation and viscous dissipation. Very recently, the investigation of thermophoresis and Brownian motion effects on MHD radiative flow of Casson fluid over a moving wedge filled with gyrotactic microorganisms is investigated by Raju et al.[27]

It is noted that very inadequate attention has been paid to study the chemical reaction effect in flow over stretching surfaces which is useful in many industrial applications processes including ceramics manufacturing, processing of food, production of polymer, ventilation, evaporation, and transfer of energy in a cooling tower and the flow in a desert cooler. The chemical reaction effect on magnetohydrodynamic flow of couple stress fluid over a nonlinearly stretching surface is examined by Khan et al.[28] Yazdi et al.[29] considered the magnetohydrodynamic liquid slip flow over a permeable non-linear stretching sheet with chemical reaction. The nanofluid flow over power-law stretching sheet under the influence of uniform magnetic field and chemical reaction was studied by Hayat et al.[30] Kiran Kumar and Varma[31] examined the effects of heat source/sink, thermal radiation, and chemical reaction on magnetohydrodynamic slip flow of nanofluid over a nonlinear permeable sheet.

In view of all the above mentioned papers, the intention of the present investigation is to study the heat and mass transfer nanofluid flow through porous medium over a slendering stretching sheet with the effects of variable

magnetic field, viscous dissipation and thermal radiation and first order chemical reactions. The series solutions for velocity, temperature, and concentration are computed by using Matlab bvp4c package. The effects of the governing parameters on the flow, heat and mass transfer aspects are discussed and presented in tables and graphs.

2. MATHEMATICAL FORMULATION

We consider a steady, electrically conducting nanofluid flow caused by a nonlinear stretching sheet coinciding with the plane $y = 0$ in a porous medium with viscous dissipation and thermal radiation. The coordinate system is considered as, x-axis is taken along the sheet and y-axis perpendicular to the sheet. The geometry of the problem is shown in Figure 1. Two equal and opposite forces are applied along the x-axis. So that the wall is stretched keeping the origin fixed. The fluid is assumed to be a gray, absorbing, emitting but non scattering medium at temperature T_∞ and concentration C_∞. The velocity stretching surface is $U_w = U_0(x+b)^m$, where the reference velocity is U_0. It is assumed that the stretching sheet is not flat in which it is specified as $y = A(x+b)^{(1-m)/2}$, where the constant A is very small in order that the sheet is sufficiently thin and m is the velocity power index. We must observe that our problem is valid for $m \neq 1$ only, because for $m = 1$, the problem is reduced to flat sheet. The radiative heat flux is described by using Rosseland approximation in the energy equation. A variable magnetic field $B(x) = B_0(x+b)^{(m-1/2)}$ acts in a transverse direction to the flow, also, the non-uniform permeability of the medium can be taken as the form $K = k'(x+b)^{1-m}$, and dimensional chemical reaction $Kr = K_0(x+b)^{1-m}$, where B_0 is the magnetic field strength, k' is the permeability of the porous medium and K_0 is the chemical reaction coefficient.

According to the above assumptions, the steady boundary layer equations of momentum, energy and concentration are given by

$$\frac{\partial u}{\partial x} + \frac{\partial v}{\partial y} = 0 \tag{1}$$

$$u\frac{\partial u}{\partial x} + v\frac{\partial v}{\partial y} = \upsilon\frac{\partial^2 u}{\partial y^2} - \frac{\sigma B^2(x)}{\rho_f}u - \frac{\upsilon}{k^1}u \tag{2}$$

$$u\frac{\partial T}{\partial x} + v\frac{\partial T}{\partial y} = \alpha\frac{\partial^2 T}{\partial y^2} + \tau\left\{D_B\frac{\partial C}{\partial y}\frac{\partial T}{\partial y} + \frac{DT}{T_\infty}\left(\frac{\partial T}{\partial y}\right)^2\right\} + \frac{\upsilon}{c_p}\left(\frac{\partial u}{\partial y}\right)^2 - \frac{1}{(\rho c_p)_f}\frac{\partial q_r}{\partial y} \tag{3}$$

$$u\frac{\partial C}{\partial x} + v\frac{\partial C}{\partial y} = D_B\frac{\partial^2 C}{\partial y^2} + \frac{D_T}{T_\infty}\frac{\partial^2 T}{\partial y^2} - K_0(C - C_\infty) \tag{4}$$

The associated boundary conditions are

$$\begin{gathered} u(x, A(x+b)^{(1-m)/2}) = U_w + \lambda_1\frac{\partial u}{\partial y}, \\ v(x, A(x+b)^{(1-m)/2}) = 0, \\ T(x, A(x+b)^{(1-m)/2}) = T_w(x), \\ C(x, A(x+b)^{(1-m)/2}) = C_w(x) \quad (\text{where } m \neq 1), \\ u(x,\infty) = 0, \quad T(x,\infty) = 0, \quad C(x,\infty) = 0 \end{gathered} \tag{5}$$

where (u, v) are the velocity components along the (x, y) directions, respectively. υ is the kinematic viscosity, c_p is the specific heat at constant pressure, ρ_f is the base fluid density, α_m is the thermal diffusivity, $\tau(=(\rho C)_f/(\rho C)_p)$ is the ratio between the effective heat capacity of the nanoparticle material and heat capacity of the fluid, D_B is the Brownian diffusion coefficient. D_T is the thermophoresis diffusion coefficient and λ_1 is the coefficient of the slip having dimension of length. We assumed that λ_1 is of the form $\lambda_1 = (x+b)^{(1-m)/2}$.

The radiative heat flux q_r is given by

$$q_r = \frac{-4\sigma^*}{3k^*}\frac{\partial T^4}{\partial y} \tag{6}$$

Where k^* is the mean absorption coefficient, σ^* is the Stefan-Boltzmann constant and the linear temperature function T^4 is expanded by using Taylors series expansion in terms of T_∞ as

$$T^4 = 4T_\infty^3 T - 3T_\infty^4 \tag{7}$$

In the view of Eqs. (6) and (7), Eq. (2) can be reduced as

$$u\frac{\partial T}{\partial x} + v\frac{\partial T}{\partial y} = \alpha\frac{\partial^2 T}{\partial y^2} + \tau\left\{D_B\frac{\partial C}{\partial y}\frac{\partial T}{\partial y} + \frac{DT}{T_\infty}\left(\frac{\partial T}{\partial y}\right)^2\right\} + \frac{\upsilon}{c_p}\left(\frac{\partial u}{\partial y}\right)^2 + \frac{16\sigma^* T_\infty^3}{3(\rho C_P)_f k^*}\frac{\partial^2 T}{\partial y^2} \tag{8}$$

We choose the wall temperature and concentration in special form as

$$T_w = T_\infty + T_0(x+b)^{(1-m)/2}, \quad \text{and} \tag{9}$$

$$C_w = C_\infty + C_0(x+b)^{(1-m)/2} \quad (\text{where } m \neq 1) \tag{10}$$

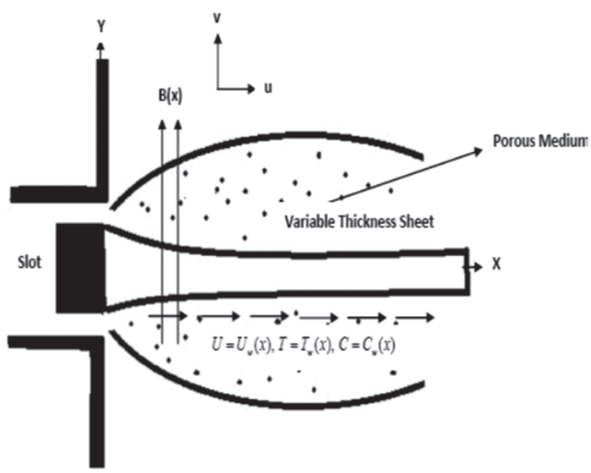

Fig. 1. Physical model and co-ordinate system.

ARTICLE

3. METHOD OF SOLUTION

Introducing the following similarity transformations (see Anjali Devi and Prakash[25] and Khader and Megahed[32])

$$\eta = y\sqrt{U_0\frac{(m+1)}{2}((x+b)^{(1-m)/2})},$$

$$\psi(x,y) = y\sqrt{\upsilon U_0\frac{2}{(m+1)}((x+b)^{m+1})}f(\eta),$$

$$\theta(\eta) = \frac{T-T_\infty}{T_w(x)-T_\infty}, \quad \phi(\eta) = \frac{C-C_\infty}{C_w(x)-C_\infty}$$

Where ψ is the stream function and is defined as $u = \partial\psi/\partial y$, $v = -\partial\psi/\partial x$, so the continuity Eq. (1) is identically satisfied.

Using these similarity variables in Eqs. (2)–(4) transformed boundary layer equations are given by

$$f''' + ff'' - \left(\frac{2m}{m+1}\right)f'^2 - \left(M + \frac{1}{K}\right)f' = 0 \tag{11}$$

$$\frac{1}{\Pr}\left(1+\frac{4R}{3}\right)\theta'' + Nb\phi'\theta' + Nt\theta'^2 + Ecf''^2 + f\theta' = 0 \tag{12}$$

$$\phi'' + Lef\phi' + \frac{Nt}{Nb}\theta'' - LeKr\phi = 0 \tag{13}$$

The corresponding boundary conditions are

$$\begin{gathered} f(\alpha) = \alpha\left(\frac{1-m}{1+m}\right)[1+\lambda f''(\alpha)], \\ f'(\alpha) = 1+\lambda f''(\alpha), \quad \theta(\alpha) = 1, \quad \phi(\alpha) = 1 \\ f'(\infty) = 0, \quad \theta(\infty) = 0, \quad \phi(\infty) = 0 \end{gathered} \tag{14}$$

Where $\alpha = A\sqrt{U_0(m+1)/(2\upsilon)}$ is a thickness parameter of the wall and $\eta = \alpha = A\sqrt{U_0(m+1)/(2\upsilon)}$ indicates the plate surface and $\lambda = A\sqrt{U_0(m+1)/(2\upsilon)}$ is the slip velocity parameter. Equations (11)–(13) with boundary conditions (14) is a nonlinear differential equation with a domain $[\alpha, \infty)$. In order to assist the computation and change the domain to become $[0, \infty)$, we define $F(\xi) = F(\eta-\alpha) = f(\eta)$, $\Theta(\xi) = \Theta(\eta-\alpha) = \theta(\eta)$ and $\Phi(\xi) = \Phi(\eta-\alpha) = \phi(\eta)$.

In the view of above transformations the Eqs. (11)–(14) become

$$F''' + FF'' - \left(\frac{2m}{m+1}\right)F'^2 - \left(M + \frac{1}{K}\right)F' = 0 \tag{15}$$

$$\frac{1}{\Pr}\left(1+\frac{4R}{3}\right)\Theta'' + Nb\Phi'\Theta'' + Nt\Theta'^2 + EcF''^2 + F\Theta' = 0 \tag{16}$$

$$\Phi'' + LeF\Phi' + \frac{Nt}{Nb}\Theta'' - LeKr\Phi = 0 \tag{17}$$

$$\begin{gathered} F(0) = \alpha\left(\frac{1-m}{1+m}\right)[1+\lambda F''(0)], \\ F'(0) = 1+\lambda F''(0), \quad \Theta(0) = 1, \quad \Phi(0) = 1 \\ F'(\infty) = 0, \quad \Theta(\infty) = 0, \quad \Phi(\infty) = 0 \end{gathered} \tag{18}$$

where the prime indicates differentiation with respect to ξ, $\Pr = \upsilon/\alpha$ is the Prandtl number, $Le = \alpha/D_B$ is the Lewis number, $Nb = (\rho C)_p D_B(C_w - C_\infty)/((\rho C)_p\upsilon)$ is the Brownian motion parameter, $Nt = (\rho C)_p D_T(T_w - T_\infty)/((\rho C)_f T_\infty\upsilon)$ is the thermophoresis parameter, $M = 2\sigma B_0^2/(U_0(m+1)\rho_f)$ is the magnetic field parameter, $Ec = U_w^2/(c_p(T_w - T_\infty))$ is the Eckert number, $R = 4\sigma^* T_\infty^3/(kk^*)$ is the radiation parameter, $K = U_0(1+m)k'/(2\upsilon)$ is the permeability parameter, $Kr = 2K_0/(U_0(m+1))$ is the chemical reaction parameter.

The physical quantities of interest, the friction factor coefficient Cf, reduced Nusselt number Nu_x and reduced Sherwood number Sh_x are defined as

$$\begin{gathered} Cf = -2\sqrt{\frac{m+1}{2}}Re_x^{-1/2}F''(0), \quad Nu_x = \frac{(x+b)q_w}{k(T_w(x)-T_\infty)}, \\ Sh_x = \frac{(x+b)q_m}{k(C_w(x)-C_\infty)} \end{gathered} \tag{19}$$

Where k, q_w, q_m are the nanofluid thermal conductivity, the heat and mass fluxes at the surface, respectively, given by

$$q_w = -k\left[\frac{\partial T}{\partial y}\right]_{y=A(x+b)^{(1-m)/2}}, \quad q_m = -D_B\left[\frac{\partial C}{\partial y}\right]_{y=A(x+b)^{(1-m)/2}} \tag{20}$$

$$\begin{aligned} Nu_x &= -\frac{(x+b)(\partial T/\partial y)_{y=A(x+b)((1-m)/2)}}{(T_w(x)-T_\infty)} \\ &= -\sqrt{\frac{m+1}{2}}Re_x^{1/2}\Theta'(0) \end{aligned} \tag{21}$$

$$\begin{aligned} Sh_x &= -\frac{(x+b)(\partial C/\partial y)_{y=A(x+b)((1-m)/2)}}{(C_w(x)-C_\infty)} \\ &= -\sqrt{\frac{m+1}{2}}Re_x^{1/2}\Phi'(0) \end{aligned} \tag{22}$$

where $Re_x = U_w X/\upsilon$ is the local Reynolds number and $X = (x+b)$.

4. RESULTS AND DISCUSSION

The set of Eqs. (15)–(17) with boundary conditions (18) has no exact analytical solutions, they are numerically solved by using Matlab bvp4c package. These equations are non-linear and coupled ordinary differential equations (ODE's). The results are excellent agreement with the existing results of Fang et al.[33] and Khader and Megahed.[32] We have used the values $m = 0.2$, $M = 1$, $\alpha = 0.2$, $\lambda = 0.2$, $K = 1$, $Nb = 0.2$, $Nt = 0.2$, $Le = 2$, $R = 0.2$, $Kr = 0.2$, $\Pr = 7.02$, and $Ec = 0.1$ throughout our analysis.

Figures 2–4 are dedicated to study the change in velocity, temperature and concentration profiles for increasing values of magnetic field parameter M. Obviously, we

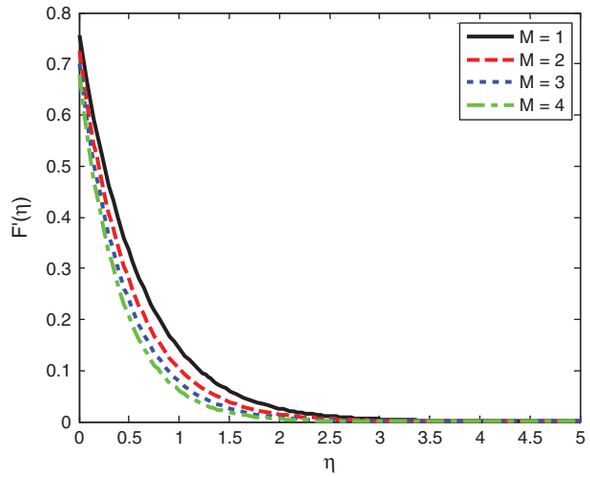

Fig. 2. Velocity profiles for various values of M.

found the reduction in velocity with the rising of M (see Fig. 2). This is because; in the presence of applied magnetic field there arises a retardation force known as Lorentz force, which has a tendency to decelerate the fluid motion within the boundary layer. Hence, we conclude that the stronger magnetic field causes to reduce the momentum boundary layer thickness. From Figure 3, it is noticed that the temperature profiles increases with increasing values of M. This is caused by additional work expended in dragging the nanofluid in the boundary layer against the action of the Lorentz force and energy is dissipated as thermal energy which heats the nanofluid. The same trend is observed on concentration profiles (see Fig. 4).

Figures 5–7 demonstrate the effect of permeability parameter K on velocity, temperature and concentration fields. It is observed the improvement in fluid velocity with rising values of K due to less friction force. More accurately, increasing K reduces fluid friction with channel

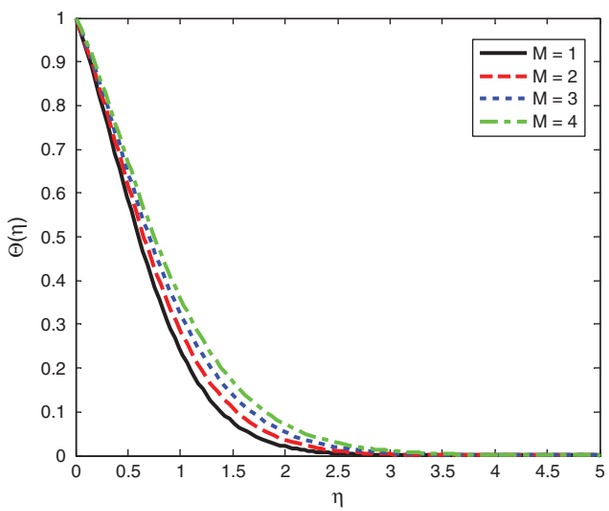

Fig. 3. Temperature profiles for various values of M.

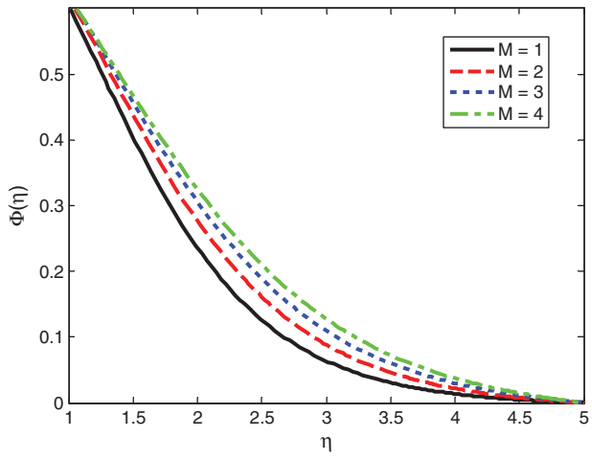

Fig. 4. Concentration profiles for various values of M.

wall and velocity enhances. Conversely, a raise in the K declines the fluid flow. Due to this reason we noticed a decrease in the fluid temperature profiles. Further, we have seen that the thickness of the solutal boundary layer decreases with K.

Figure 8 depicts the effect of non-linear stretching parameter m on stream wise velocity. From this figure it is seen that, an increase in m leads to decline in velocity. Also, the momentum boundary layer thickness decreases with increasing non-linear stretching parameter m. Figure 9 shows the effect of m on temperature profiles. The presence of m leads to rise in the thermal boundary layer thickness.

The influence of wall thickness parameter α on velocity, temperature and concentration distributions are shown in Figures 10–12. The fluid velocity fields are minimized with an improved value of α. This is because for higher value of α the boundary layer becomes thicker. From Figure 11 it can be seen that, an increase in the wall thickness parameter results in decrease the fluid temperature.

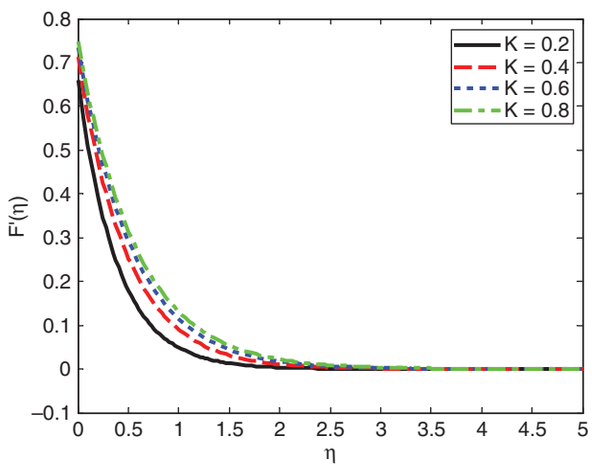

Fig. 5. Velocity profiles for various values of K.

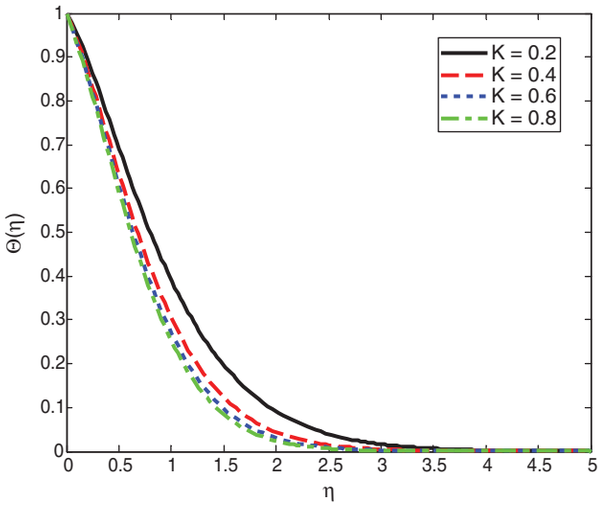

Fig. 6. Temperature profiles for various values of K.

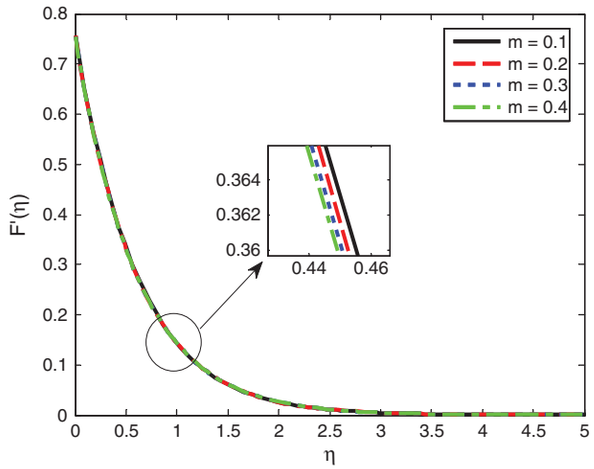

Fig. 8. Velocity profiles for various values of m.

The same phenomenon is observed on concentration profiles (see Fig. 12).

Figure 13 displays the influence of velocity slip parameter λ on velocity distributions. It is observed that the slip at the surface wall raises with an increase in λ, and consequently reaches to a less amount of penetration because of the stretching surface into the fluid. It is obvious from figure that the component of the fluid velocity at the wall decreases with the improved values of λ and declines asymptotically to zero at the edge of the momentum boundary layer. Thus, the slip parameter λ depreciates the momentum boundary layer thickness.

The temperature profiles for various values of Brownian motion Nb is depicted in Figure 14. It is described that the nanofluid temperature increases with the rising values of Nb. Physically, Nanoparticles motion plays a pivotal role in thermal conduction. Because of the intensified chaotic motion of the nanoparticles the kinetic energy of the particles is improved which as a result boost up the nanofluid temperature. Therefore, increasing Nb firmly accelerate temperature values throughout the regime.

The influence of thermophoresis parameter Nt on temperature distribution is revealed in Figure 15. Physically, thermophoresis parameter causes high temperature gradients. These in turn result in high temperature distributions within the nanofluid flow.

Figure 16 shows the variation of Radiation parameter R on temperature distribution. It is noticed that, the nanofluid temperature accelerates for growing values of R. This is due to the fact that an increase in R provides more heat to fluid that causes an improvement in the temperature as well as boundary layer thickness.

The influence of Eckert number Ec on temperature distribution is shown in Figure 17. It can be seen, the effect of Ec on boundary layer thickness is insignificant at Richardson numbers lower than unity. The motivation which might be associated to this is that natural convection is closer to forced convection flow and the order of magnitude of inertia forces on velocity is more than shear forces, while

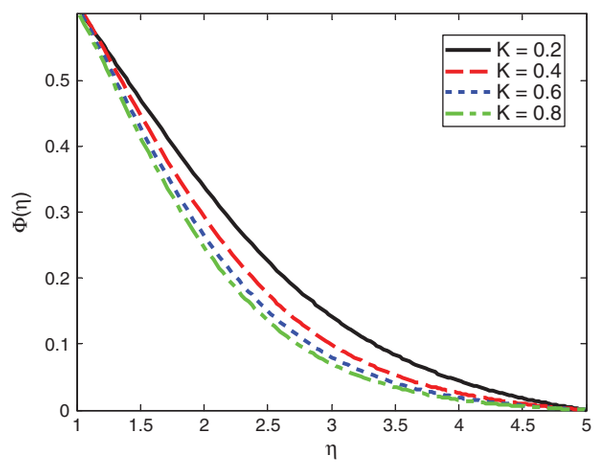

Fig. 7. Concentration profiles for various values of K.

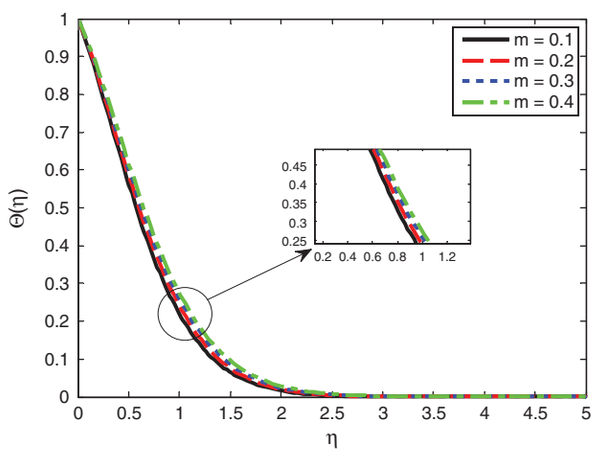

Fig. 9. Temperature profiles for various values of m.

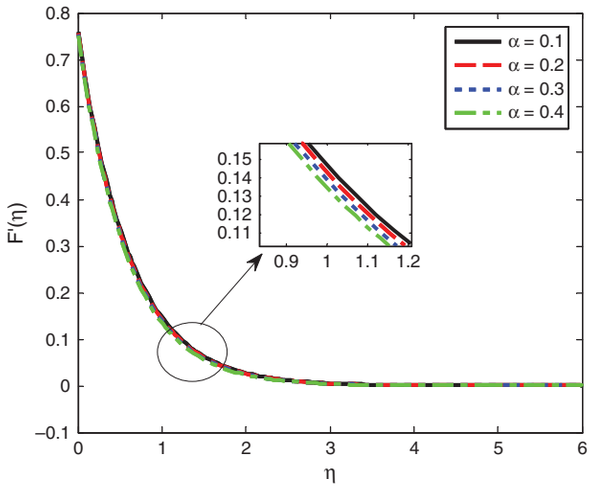

Fig. 10. Velocity profiles for various values of α.

at Richardson numbers higher than unity, the improvement of Ec motivates the boundary layer thickness.

Figure 18 illustrates the dimensionless concentration distribution for various values of chemical reaction parameter Kr. It is evident that an increase in Kr depreciates the fluid concentration. Particularly, if the strength of the chemical reaction is higher than the thermophoresis particle deposition then the nanoparticle volume fraction of the fluid gradually changes from higher value to the lower value. The interesting result is the large distortion of the nanoparticle volume field. This type of physical behavior is caused by the combined effects of the strength of the Brownian motion and thermophoresis particle deposition.

Figure 19 gives the effect of Lewis number Le on concentration profiles. The dimensionless concentration profiles are decreases significantly with increasing Lewis number. In fact, Le assert the relative contribution of thermal diffusion rate (α) to species diffusion rate (D_B) within the boundary layer regime. Also, the improved values of Le will suppress concentration values i.e., reduce the nanoparticle species diffusion (D_B).

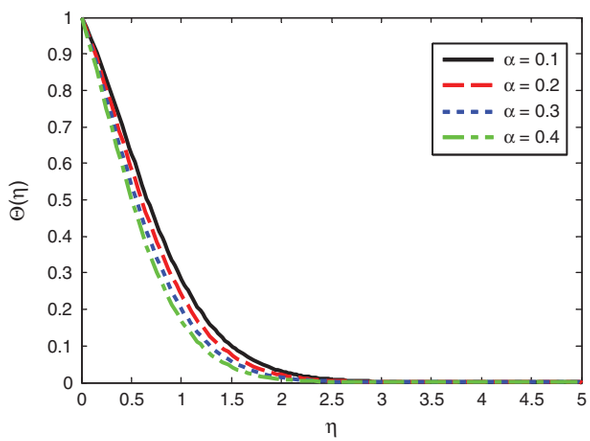

Fig. 11. Temperature profiles for various values of α.

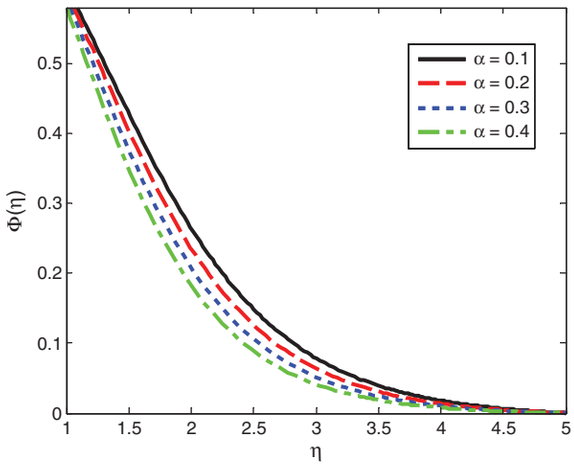

Fig. 12. Concentration profiles for various values of α.

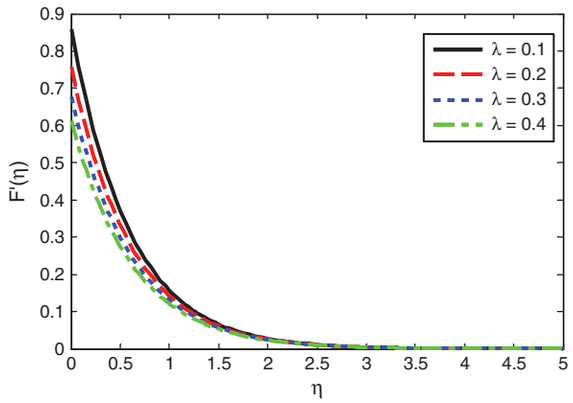

Fig. 13. Velocity profiles for various values of λ.

Figure 20 exhibits the influence of Prandtl number Pr on temperature. It is noticed that, the nanofluid temperature insignificantly reduced with increasing values of Pr. This is because of the fact that a higher Pr has relatively low

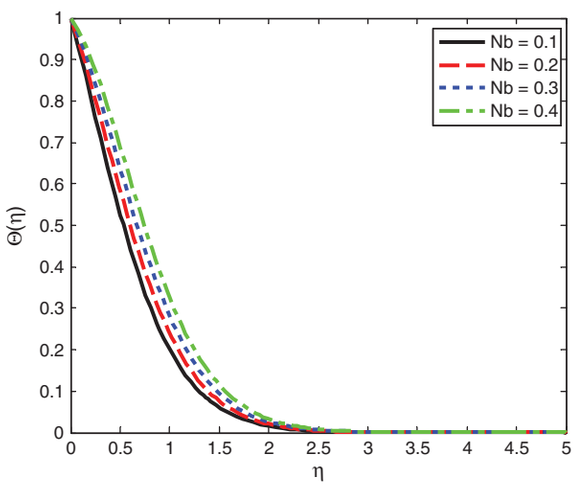

Fig. 14. Temperature profiles for various values of Nb.

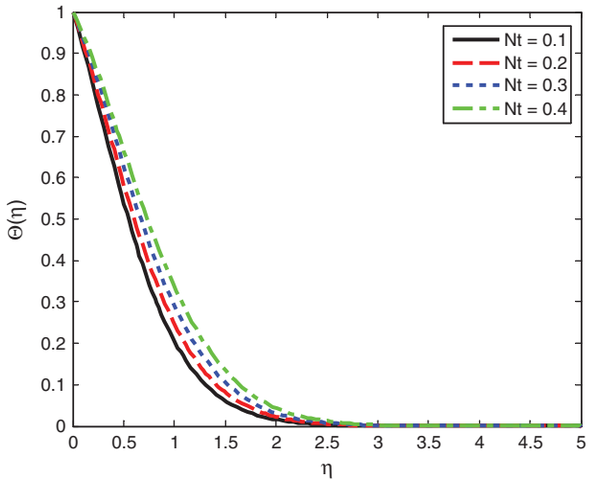

Fig. 15. Temperature profiles for various values of Nt.

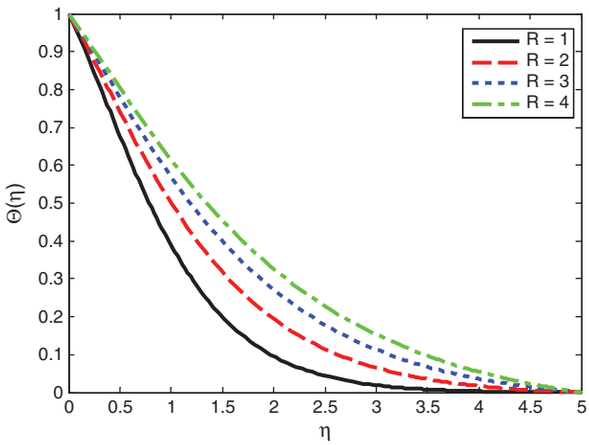

Fig. 16. Temperature profiles for various values of R.

thermal conductivity, which reduces conduction and thus temperature decreases.

We have compared the skin friction coefficient $-f''(0)$ with previous published results by Khader and Megahed[32]

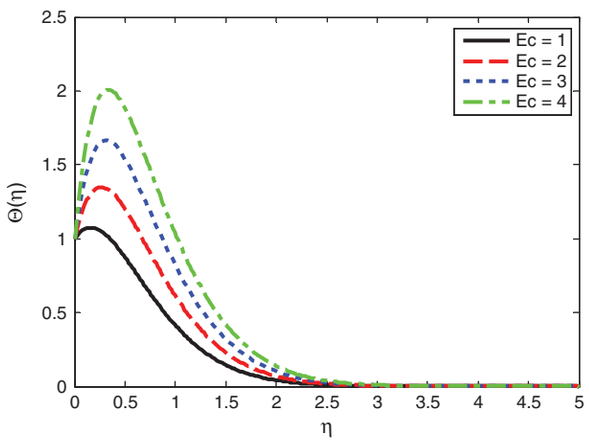

Fig. 17. Temperature profiles for various values of Ec.

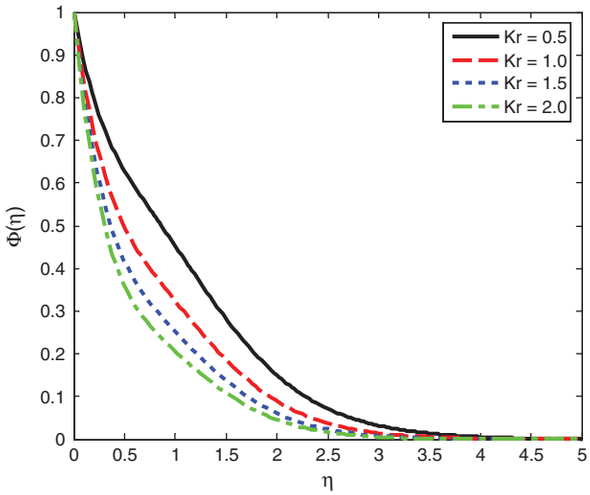

Fig. 18. Concentration profiles for various values of Kr.

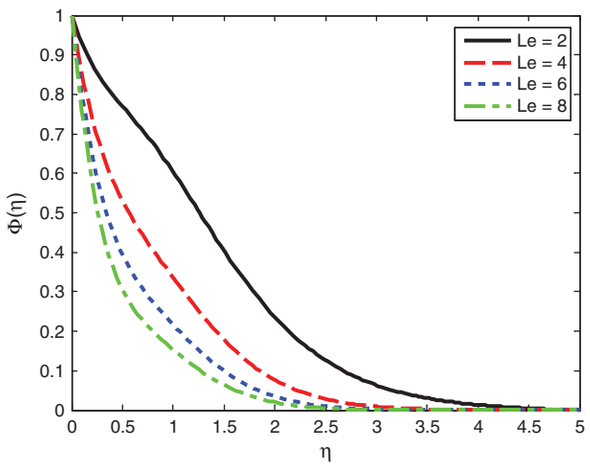

Fig. 19. Concentration profiles for various values of Le.

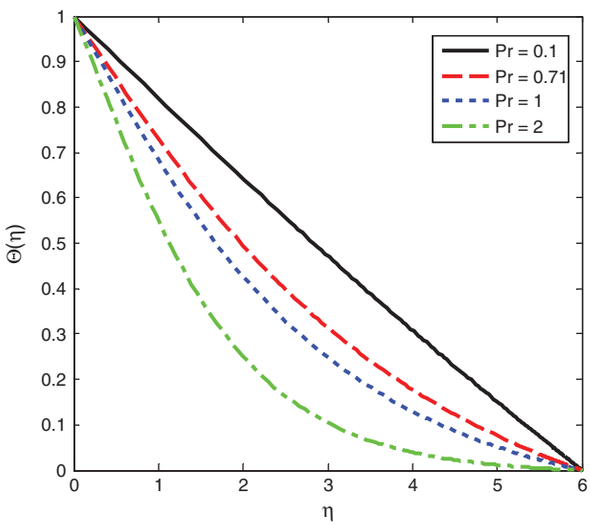

Fig. 20. Temperature profiles for various values of Pr.

Table I. Comparison of the numerical values of $-f''(0)$ for $\alpha=0.5$ with $\lambda=M=Nt=Nb=R=Le=Kr=Ec=0$, $K\to\infty$.

m	Fang et al.[33]	Khader and Megahed[32]	Present work
10.00	1.0603	1.0603	1.060729
9.00	1.0589	1.0588	1.059325
7.00	1.0550	1.0551	1.055466
5.00	1.0486	1.0486	1.049050
3.00	1.0359	1.0358	1.036336
2.00	1.0234	1.0234	1.023860
1.00	1.0000	1.0000	1.000483
0.50	0.9799	0.9798	0.980384
0.00	0.9576	0.9577	0.957924
−0.50	1.1667	1.1666	1.666822

Table II. Comparison of the numerical values of $-f''(0)$ for $\alpha=0.25$ with $M=Nt=Nb=R=Le=Kr=Ec=0$, $K\to\infty$.

m	Fang et al.[33]	Khader and Megahed[32]	Present work
10.00	1.1433	1.1433	1.143716
9.00	1.1404	1.1404	1.140710
7.00	1.1323	1.1322	1.132689
5.00	1.1186	1.1186	1.119092
3.00	1.0905	1.0904	1.090929
2.00	1.0000	1.0000	1.000483
1.00	0.9338	0.9337	0.934325
0.50	0.78439	0.7843	0.784773
0.00	0.5000	0.5000	0.500417
−0.50	0.0833	0.0832	0.083651

and Fang et al.[33] in Tables I–III respectively, to validate the exactness of present results. Effects of dissipation parameter Ec on friction factor, local Nusselt number and local Sherwood number are presented in Table IV. It is clear that the friction factor increases with an increases in α and m while it decreases with the increasing values of λ. The magnitude of heat transfer coefficient depreciates with the rising values of λ, m, R, Kr and Le, but the opposite trend

Table III. Comparison of the numerical values of $-f''(0)$ for various values of α, λ and m when $M=Nt=Nb=R=Le=Kr=Ec=0$, $K\to\infty$.

λ	α	m	Khader and Megahed[32]	Present work
0.0	0.2	0.5	0.924828	0.924822
0.2	0.2	0.5	0.728201	0.728192
0.5	0.2	0.5	0.561082	0.561070
0.2	0.0	0.5	0.707579	0.707569
0.2	0.25	0.5	0.733395	0.733387
0.2	0.5	0.5	0.759570	0.759563
0.2	1.0	0.5	0.812747	0.812743
0.2	0.0	5.0	0.890165	0.890156
0.2	0.25	5.0	0.850600	0.850558
0.2	0.5	5.0	0.812508	0.812494
0.2	1.0	5.0	0.741247	0.741230
0.2	0.2	0.0	0.611306	0.611299
0.2	0.2	0.5	0.728201	0.728192
0.2	0.2	2.0	0.819489	0.819478
0.2	0.2	5.0	0.858401	0.858389

Table IV. Numerical values of skin friction coefficient, local Nusselt number and local Sherwood number for various values of λ, α, m, R, Kr and Le.

λ	α	m	R	Kr	Le	$F''(0)$	$-\Theta'(0)$	$-\Phi'(0)$
0.1	0.2	0.5	2.0	0.5	2	1.425898	0.411195	1.278733
0.2						1.231759	0.388098	1.247931
0.3						1.086623	0.367227	1.225688
0.2	0.25					1.235307	0.400023	1.253930
	0.5					1.253046	0.461007	1.281942
	1.0					1.288475	0.588481	1.329472
		0.2				1.217572	0.443620	1.271360
		0.4				1.227757	0.403728	1.254836
		0.6				1.235227	0.374583	1.241743
			1.0			1.231759	0.437184	1.251208
			2.0				0.388098	1.247931
			3.0				0.349068	1.253108
				1.0		1.231759	0.376013	1.671477
				2.0			0.365422	2.257839
				3.0			0.360238	2.702842
				1.0		1.231759	0.411996	0.774840
					2.0		0.388098	1.247931
					3.0		0.376495	1.608370

is for increasing value of α. The rate of mass transfer coefficient decreases with an raise in λ, m and R whereas it increases for increasing values of α, Kr and Le. Also no effect of R, Kr and Le is seen on skin friction coefficient.

5. CONCLUSIONS

The magnetohydrodynamic boundary layer nanofluid flow through porous medium over a variable thickness sheet with viscous dissipation, thermal radiation and chemical reaction have been investigated numerically. The impact of various flow parameters are presented through graphs and tables.

The main remarks are as follows:

1. The friction factor coefficient boost up with the improved values of α and m while it decreases with the increasing values of λ.
2. The rate of heat and mass transfer coefficients decreases with increasing R.
3. The stream wise velocity of the nanofluid decrease with increase in slip parameter λ and non-linear stretching parameter m.
4. Radiation parameter, viscous dissipation parameter and thermophoresis parameter enhances the nanofluid temperature.
5. The increase in Lewis number Le reduces the species concentration.
6. Rise in destructive Kr reduces the solutal boundary layer thickness.

References and Notes

1. L. J. Crane, *Z. Angew. Math. Phys.* 21, 645 (**1970**).
2. B. K. Dutta, P. Roy, and A. S. Gupta, *Int. Commun. Heat Mass Transf.* 12, 89 (**1985**).

3. S. U. S. Choi, Enhancing Thermal Conductivity of Fluids with Nanoparticles Developments Applications of Non-Newtonian Flows, edited by D. A. Signine and H. P. Wang, ASME, New York **(1995)**, Vol. 66, pp. 99–105.
4. J. Buogiorno, *ASME J. Heat Transfer* 128, 240 **(2006)**.
5. J. Buongiorno, et al., *J. Appl. Phys.* 106, 1 **(2009)**.
6. S. A. Angayarkanni and J. Philip, *Adv. Colloid Interface Sci.* 225, 146 **(2015)**.
7. S. A. Angayarkanni and J. Philip, *J. Phys. Chem. C* 118, 13972 **(2014)**.
8. P. D. Shima and J. Philip, *Ind. Eng. Chem. Res.* 53, 980 **(2014)**.
9. S. A. Angayarkanni and J. Philip, *J. Appl. Phys.* 118, 1 **(2015)**.
10. M. A. A. Hamad and M. Ferdows, *Appl. Math. Mech. Eng.* 33, 923 **(2012)**.
11. P. Rana and R. Bhargava, *Commun. Nonlinear Sci. Numer. Simul.* 17, 212 **(2012)**.
12. K. Das, *Journal of the Egyptian Mathematical Society* 23, 451 **(2015)**.
13. S. Shaw, P. K. Kameswaran, and P. Sibanda, *Boundary Value Problems* 2016, 1 **(2016)**.
14. P. Ganesan and G. Palani, *Int. J. Heat Mass Transf.* 47, 4449 **(2004)**.
15. F. Mabood, W. A. Khan, and A. I. M. Ismail, *Journal of Magnetism and Magnetic Materials* 374, 569 **(2015)**.
16. K. Vajravelu, K. V. Prasad, and H. Vaidya, *Communications in Numerical Analysis* 2016, 17 **(2016)**.
17. M. S. Abel, K. A. Kumar, and R. Ravikumara, *Engineering* 3, 285 **(2011)**.
18. S. P. Anjali Devi and M. Prakash, *Journal of the Nigerian Mathematical Society* 34, 318 **(2015)**.
19. K. Y. Yohannes and B. Shankar, *Carib. J. SciTech.* 1, 1 **(2013)**.
20. A. Ahmed, Khidir, and P. Sibanda, *Journal of Porous Media* 17, 391 **(2014)**.
21. P. Durga Prasad, R. V. M. S. S. Kiran Kumar, and S. V. K. Varma, MHD free convection and heat transfer enhancement of nanofluids through a porous medium in the presence of variable heat flux **(2017)**, Vol. 6, pp. 496–504.
22. R. Cortell, *Phys. Lett. A* 372, 631 **(2008)**.
23. P. Rana, R. Dhanai, and L. Kumar, *Ain Shams Engineering Journal* **(2015)**, Article in press.
24. D. Pal, G. Mandal, and K. Vajravelu, *Int. J. Heat Mass Transfer* 65, 481 **(2013)**.
25. S. P. Anjali Devi and M. Prakash, *J. Braz. Soc. Mech. Sci. Eng.* 38, 423 **(2016)**.
26. V. Nagendramma, R. V. M. S. S. Kiran Kumar, and P. Durga Prasad, *J. Nanofluids* 5, 817 **(2016)**.
27. C. S. K. Raju, *Adv. Powder Technol.* 28, 575 **(2017)**.
28. N. A. Khan, F. Riaz, and F. Sultan, *European Physical Journal Plus* 129, 1 **(2014)**.
29. M. H. Yazdi, S. Abdullah, I. Hashim, and K. Sopian, *Int. J. Heat Mass Transfer* 54, 3214 **(2011)**.
30. T. Hayat, M. Rashid, M. Imtiaz, and A. Alsaedi, *AIP Advances* 5, 1 **(2015)**.
31. R. V. M. S. S. Kiran Kumar and S. V. K. Varma, *J. Nanofluids* 6, 48 **(2017)**.
32. M. M. Khader and A. M. Megahed, *Eur. Phys. J. Plus* 128, 1 **(2013)**.
33. T. Fang, J. Zhang, and Y. Zhong, *Appl. Math. Comput.* 218, 7241 **(2012)**.